AIChE

Design of Mixed Conducting Ceramic Membranes/Reactors for the Partial Oxidation of Methane to Syngas

Xiaoyao Tan
School of Chemical Engineering, Shandong University of Technology, Zibo, PR China, 255049

K. Li
Dept. of Chemical Engineering and Technology, Imperial College London, South Kensington, London SW7 2AZ, U.K.

DOI 10.1002/aic.11873
Published online July 16, 2009 in Wiley InterScience (www.interscience.wiley.com).

The performance of mixed conducting ceramic membrane reactors for the partial oxidation of methane (POM) to syngas has been analyzed through a two-dimensional mathematical model, in which the material balance, the heat balance and the momentum balance for both the shell and the tube phase are taken into account. The modeling results indicate that the membrane reactors have many advantages over the conventional fixed bed reactors such as the higher CO selectivity and yield, the lower heating point and the lower pressure drop as well. When the methane feed is converted completely into product in the membrane reactors, temperature flying can take place, which may be restrained by increasing the feed flow rate or by lowering the operation temperature. The reaction capacity of the membrane reactor is mainly determined by the oxygen permeation rate rather than by the POM reaction rate on the catalyst. In order to improve the membrane reactor performance, reduction of mass transfer resistance in the catalyst bed is necessary. Using the smaller membrane tubes is an effective way to achieve a higher reaction capacity, but the pressure drop is a severe problem to be faced. The methane feed velocity for the operation of mixed conducting membrane reactors should be carefully regulated so as to obtain the maximum syngas yield, which can be estimated from their oxygen permeability. The mathematical model and the kinetic parameters have been validated by comparing modeling results with the experimental data for the $La_{0.6}Sr_{0.4}Co_{0.2}Fe_{0.8}O_{3-\alpha}$ (LSCF) membrane reactor.
 AIChE J, 55: 2675–2685, 2009
Keywords: mixed conducting membrane, perovskite, partial oxidation of methane, membrane reactor, modeling

Introduction

Partial oxidation of methane (POM) is a promising process for syngas production due to its favorable product distribution, i.e., H_2 to CO ratio = 2:1, and the mild thermal effect ($CH_4 + 1/2O_2 = CO + 2H_2 - 35.6$ kJ). In conventional POM processes, air is usually used as the oxidant and

Correspondence concerning this article should be addressed to K. Li at Kang.Li@Imperial.ac.uk

subsequently, the costly nitrogen separation from syngas product mixtures has to be performed. Pure oxygen may be used as the oxidant to avoid nitrogen separation, but oxygen production by either cryogenic distillation or pressure swing adsorption (PSA) is extremely expensive. In recent years, considerable research has been focused on the integration of oxygen permeable ceramic membranes, which are prepared from mixed oxygen ion and electron conducting ceramics, with POM reactions.[1–10] In such mixed conducting ceramic membrane reactors, methane and air are respectively introduced into the opposite sides of the membrane. Oxygen is permeated through the membrane under the oxygen partial pressure gradient into the methane side where POM reactions take place with presence of catalysts. As the membrane is 100% permselective to oxygen, nitrogen would not be present in the product mixture and the post separation of nitrogen can be avoided. In addition, the local oxygen concentration can be maintained at a relatively low and uniform value due to the discrete addition of the oxygen through the membrane. As a result, not only the high CO selectivity and methane conversion can be achieved, but also the excessive temperature excursion can be avoided.

The mixed conducting ceramic membrane reactors for POM can generally be found in three configurations: disc-shaped membrane reactor, tubular membrane reactor, and hollow fiber membrane reactor. In general, the disk-shaped membrane reactors give a low syngas production rate due to the limited membrane area. Also, the requirement of rigorous high-temperature sealing makes it difficult to scale up.[2–5] It is less problematic for the tubular membrane reactors,[6–8] but they are normally thick to have enough mechanical strength, which makes them unfavorable for oxygen permeation flux. Recently, the hollow fiber membrane reactors have attracted much interest due to obvious advantages over the disc and tubular membranes such as large membrane area/volume ratio and less effective membrane thickness.[9,10] However, the hollow fiber membranes have lower mechanical strength than the tubular membranes and thus are more difficult to be assembled into membrane reactors. To combine advantages of the tubular and the hollow fiber membranes, the composite membrane with a thin dense perovskite film coated on a porous substrate tube would be a good choice to obtain high POM selectivity and yields[11] as long as the thermal expansion mismatch of the coating and substrate ceramics can be minimized.

It is acknowledged that many challenges have to be faced before the commercialization of the membrane processes for syngas production by POM can be realized. First, a high temperature is essential to oxygen permeation. However, it is harmful to the POM catalysts if the temperature is too high. Second, the oxygen permeation can be promoted by reducing the membrane thickness, but preparation of thin dense ceramic membrane on a porous support is difficult and costly. In addition, the mixed conducting membranes with good stability in the POM environmental atmosphere usually possess low oxygen permeability, thus a large membrane area is expected for a high oxygen permeation rate. Modeling is a useful method to evaluate the performances of membrane reactors. From the theoretical simulations, the advantages and potential problems of membrane reactors can be deduced conveniently and rapidly. The one-dimensional

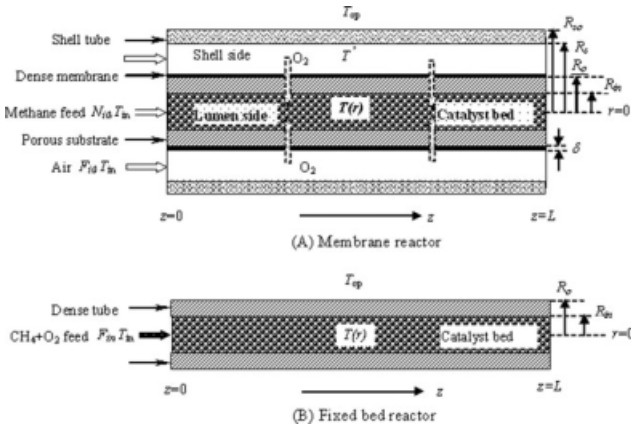

Figure 1. Schematic of (A) tubular mixed conducting ceramic membrane reactor and (B) packed bed reactor.

model was most often adopted previously because of its simplicity and ease of handling, but it fails to predict the effect of the radial transportation which could be not negligible in a large-scale membrane reactor.[12–16] Recently, the two-dimensional model was applied to POM in oxygen permeable membrane reactors, with which the effect of reactor dimensions on the POM performance was investigated.[17] In this work, not only the radial concentration and temperature gradients but also the gas volume change and the pressure drop inside the membrane reactor are all taken into account in the modeling process. The objective of the present article is to analyze the behaviors of mixed conducting ceramic membrane reactors with a more practical model so that some guidances for the design of ceramic membranes and membrane reactors for syngas production can be rationalized.

Model development

The modeling work is based on the tubular mixed conducting ceramic membrane reactor in which a membrane tube is coaxially housed in a shell tube with the inner diameter of R_s, as shown in Figure 1. The mixed conducting ceramic is coated on the porous support tube to form a dense film with a thickness of δ while a typical POM catalyst such as Ni/γ-Al_2O_3 is packed in the tube side. The whole membrane reactor is located in a tubular furnace. During operations, methane is fed into the tube side (catalyst bed) while air is introduced co-currently into the shell side of the membrane reactor.

Model equations

The following assumptions are adopted for the derivation of model equations:

1. Plug flow on both the air and the methane sides with negligible axial dispersion. This assumption is valid in the case of turbulent flow, and for large reactor length/tube diameter and tube diameter/particle diameter ratios.

2. The mass-transfer resistances in the porous support and between the gas and the membrane surfaces are negligible.

3. The radial pressure drop as well as the radial convective flow is negligible. Also, the pressure drop in the shell side is neglected.

4. The intraparticle and the interphase mass-transfer resistance can be incorporated into a global reaction kinetics model (pseudo homogeneous reaction with an effectiveness factor).

5. Ideal gas law is obeyed to both single component and gas mixture.

6. Steady state operation.

In the catalyst bed (tube side), the mass balance for each component may be given in cylindrical coordinate as:

$$\frac{\partial N_i}{\partial z} = D_{ei}\left(\frac{1}{r}\frac{\partial c_i}{\partial r} + \frac{\partial^2 c_i}{\partial r^2}\right) + \rho_s(1-\varepsilon_b) \times \sum_j \nu_{ji}\mathcal{R}_j \ (i = CH_4,\ O_2,\ CO_2,\ H_2O,\ CO,\ H_2) \quad (1)$$

with the boundary conditions:

$$r = 0,\ \frac{\partial c_i}{\partial r} = 0;\ r = R_{in},\ D_{ei}\frac{\partial c_i}{\partial r} = \frac{R_m}{R_{in}}\cdot J_i \quad (1a)$$

$$z = 0,\ N_i = N_{i0} \quad (1b)$$

where N_i is the molar flux of species i in the tube phase; c_i the species concentration; D_{ei} the effective diffusion coefficient; ρ_s the catalyst density; ε_b the void fraction of the catalyst bed; ν_{ji} the stoichiometric coefficient of species i in reaction j; (j the overall rate of reaction j, $\mathcal{R}_j = \zeta_j f_j(T', c_1^t, c_2^t, \cdots)$ in which ζ_j is the effectiveness factor of catalyst for reaction i; R_{in} the inner radius of the membrane tube; R_m the algorithm mean radius of the dense membrane, $R_m = \frac{\delta}{\ln(1+\delta/R_o)}$, in which R_o and δ are, respectively, the outer radius of the membrane tube and the thickness of the dense film; J_i is the permeation flux of gas species i through the membrane, and N_{i0} is the feed molar flux.

The component concentration, c_i is related to the molar fluxes by:

$$c_i = \frac{p}{RT}\cdot\frac{N_i}{\sum_i N_i} \quad (2)$$

where p and T are the local pressure and temperature, respectively, in the catalyst bed; and R is the ideal gas constant.

The energy balance equation in the tube side is given by:

$$\sum_i N_i C_{p,i}\frac{\partial T}{\partial z} = \lambda_{ec}\left(\frac{1}{r}\frac{\partial T}{\partial r} + \frac{\partial^2 T}{\partial r^2}\right) + \rho_s(1-\varepsilon_b)\sum_j \mathcal{R}_j(-\Delta H_j) \quad (3)$$

with the boundary conditions:

$$r = 0,\ \frac{\partial T}{\partial r} = 0;\ r = R_{in},\ \lambda_{ec}\frac{\partial T}{\partial r} = K_m(T' - T) \quad (3a)$$

$$z = 0,\ T = T_{in} \quad (3b)$$

where C_{pi} is the specific heat capacity of species i; T' the temperature of shell phase; λ_{ec} the effective thermal conductivity of the tube phase; ΔH_j the reaction heat of reaction j; K_m the overall heat transfer coefficient between the shell and the tube phases; and T_{in} is the gas feed temperature.

The pressure drop formed by the catalyst packing can be expressed by Ergun's equation:

$$\frac{dp}{dz} = -u_t\left(\frac{150\mu_g}{d_p^2}\cdot\frac{(1-\varepsilon_b)^2}{\varepsilon_b^3} + \frac{1.75\rho_g u_t}{d_p}\cdot\frac{1-\varepsilon_b}{\varepsilon_b^3}\right) \quad (4)$$

with the boundary condition:

$$z = L,\ p = p_a \quad (4a)$$

where μ_g and ρ_g are the viscosity and density of the tube gas mixture, respectively; d_p the equivalent diameter of the catalyst particle; L the effective length of the membrane reactor; p_a is the pressure at the outlet of membrane reactor, i.e, the atmospheric pressure in this work. The average superficial velocity of the lumen bulk gas, u_t is calculated by:

$$u_t = \frac{1}{\pi R_{in}^2}\cdot\sum_i\int_0^{R_{in}}\frac{N_i RT}{p}\cdot 2\pi r dr \quad (5)$$

One-dimensional model may be applied to the shell phase. So the mass and heat balance equations in the shell side may be written as:

$$\frac{dF_i}{dz} = -2\pi R_m\cdot J_i(i = N_2,\ O_2) \quad (6)$$

$$\sum_i F_i C_{pi}\frac{dT'}{dz} = K_s\cdot 2\pi R_s(T_{op} - T') - K_m\cdot 2\pi R_{in}(T' - T) - 2\pi R_m\cdot J_h \quad (7)$$

with the boundary conditions:

$$z = 0,\ F_i = F_{Air},\ T' = T_{in} \quad (8)$$

where F_i is the molar flow rate of species i in the shell phase; K_s and K_m are the overall heat transfer coefficients from the furnace tube to the shell phase, and from the shell phase to the tube phase, respectively; T_{op} is the operation temperature; J_h is the heat flux due the gas permeation from the shell side to the tube side; and F_{Air} is the air feed flow rate.

For the traditional fixed bed reactors (FBR), the methane is mixed with oxygen in advance and is then co-fed into the catalyst bed, as shown in Figure 1B. The governing equations can also be expressed by Eqs. 1, 3, and 4 but only the boundary conditions are changed as follows.

$$z = 0,\ N_i = N_{i0},\ T = T_{in} \quad (9a)$$

$$L > z > 0,\ r = 0,\ \frac{\partial c_i}{\partial r} = 0,\ \frac{\partial T}{\partial r} = 0 \quad (9b)$$

$$r = R_{in},\ \frac{\partial c_i}{\partial r} = 0, \lambda_{ec}\frac{\partial T}{\partial r} = K_m(T_{op} - T) \quad (9c)$$

Kinetic equations

The POM mechanism to syngas on the Ni/γ-Al_2O_3 catalyst can be described by the methane combustion followed by

Table 1. Kinetic Parameters for the Partial Oxidation of Methane to Syngas on Ni/γ-Al_2O_3 Catalyst

k_1, mol g^{-1} s^{-1} Pa^{-2}	$k_1 = 1.1\ \exp(-166 \times 10^3/RT)^7$
k_2, mol g^{-1} s^{-1} Pa^{-2}	$k_2 = 4.19 \times 10^{-9}\ \exp(-29 \times 10^3/RT)^7$
k_3, mol g^{-1} s^{-1} Pa^{-2}	$k_3 = 2.42 \times 10^{-9}\ \exp(-23.7 \times 10^3/RT)$
K_2, Pa^2	$\ln(K_2/10^{10}) = -\frac{22851.7}{T} + 7.682 \ln T - 4.165 \times 10^{-3}T + 3.58 \times 10^{-7}T^2 - 23.247$
K_3, Pa^2	$\ln(K_3/10^{10}) = -\frac{2.785\times10^4}{T} + 7.93 \ln T - 5.635 \times 10^{-3}T + 5.862 \times 10^{-7}T^2 - 18.93$
ΔH_1, kJ mol^{-1}	$\Delta H_1 = -4410.9 + 14.58T - 8.426 \times 10^{-3}T^2 + 3.98 \times 10^{-7}T^3$
ΔH_2, kJ mol^{-1}	$\Delta H_2 = -15915.1 + 63.867T - 34.631 \times 10^{-3}T^2 + 5.955 \times 10^{-6}T^3$
ΔH_3, kJ mol^{-1}	$\Delta H_3 = -15504.8 + 65.934T - 46.847 \times 10^{-3}T^2 + 9.748 \times 10^{-6}T^3$

both steam and carbon dioxide reforming.[18,19] The kinetic equations may be written as follows[7]:

Methane combustion:

$$CH_4 + 2O_2 \rightarrow CO_2 + 2H_2O + \Delta H_1 \quad \text{(i)}$$

$$\mathcal{R}_1 = k_1 p_{CH_4} p_{O_2} \quad (10)$$

Steam reforming:

$$CH_4 + H_2O \Leftrightarrow CO + 3H_2 + \Delta H_2 \quad \text{(ii)}$$

$$\mathcal{R}_2 = k_2 p_{CH_4} p_{H_2O}\left(1 - \frac{p_{CO} p_{H_2}^3}{K_2 p_{CH_4} p_{H_2O}}\right) \quad (11)$$

Carbon dioxide reforming:

$$CH_4 + CO_2 \Leftrightarrow 2CO + 2H_2 + \Delta H_3 \quad \text{(iii)}$$

$$\mathcal{R}_3 = k_3 p_{CH_4} p_{CO_2}\left(1 - \frac{p_{CO}^2 p_{H_2}^2}{K_3 p_{CH_4} p_{CO_2}}\right) \quad (12)$$

where k_j ($j = 1, 2, 3$) is the reaction rate constant; and K_j($j = 2, 3$) is the equilibrium constant. Values of these parameters may be obtained by fitting experimental data or calculated from the thermodynamic properties of gases, as listed in Table 1.

Oxygen permeation fluxes through the membrane tube

The mixed ionic-electronic conducting ceramic membranes are 100% permselective to oxygen, that is, no other species but oxygen can permeate through the dense membrane ($J_i(i \neq O_2) = 0$). For the perovskite membranes such as $La_{0.6}Sr_{0.4}Co_{0.2}Fe_{0.8}O_{3-\alpha}$ (LSCF) in which the electronic conductivity overwhelms the oxygen ionic conductivity,[20] the local oxygen permeation flux through the tubular membranes may be expressed by[21,22]:

$$J_{O_2} = \frac{k_r[(p'_{O_2})^{0.5} - (p_{O_2})^{0.5}]}{\frac{R_m}{R_O+\delta} \cdot p_{O_2}^{0.5} + \frac{2k_f\delta}{D_v} \cdot (p_{O_2}p'_{O_2})^{0.5} + \frac{R_m}{R_O} \cdot (p'_{O_2})^{0.5}} \quad (13)$$

where D_V is the diffusion coefficient of oxygen vacancy; k_f and k_r are, respectively, the forward and the reverse reaction rate constants of the surface exchange reaction:

$$\frac{1}{2}O_2 + V_O \overset{k_f/k_r}{\longleftrightarrow} O_O^x + 2h \quad (14)$$

The energy associated with the oxygen permeation only gives a small contribution to the total heat flux (<5%).[23] But it was also considered in the energy balance equation (Eq. 7) for the completeness of the model in our work.

Mass and heat transfer coefficients

The effective diffusion coefficient of gas species in the catalyst bed is given by[14]:

$$D_{ei} = \varepsilon_b \cdot \frac{1 - y_i}{\sum_{j \neq i} y_i / D_{i,j}} \quad (15)$$

where y_i is the molar fraction of species i, and $D_{i,j}$ is the binary diffusion coefficient between species i and j, which may be estimated by the Maxwell–Gilliland equation:

$$D_{i,j} = \frac{4.36 \times 10^{-5} T^{3/2} (1/M_i + 1/M_j)^{0.5}}{p(v_i^{1/3} + v_j^{1/3})^2} \quad (15a)$$

where M, υ are the molecular weight and the molecular volume of gas species, respectively.

Exact calculation of the effective thermal conductivity of the packed tube phase, λ_{ec} is very complicated.[8] For simplification, it is calculated in this work using a simplified expression by assuming that the catalyst bed is a pseudo homogenous phase composed by catalyst particles and gas mixture[24]:

$$\lambda_{ec} = \varepsilon_b \sum_i y_i \lambda_{gi} + (1 - \varepsilon_b)\lambda_c \quad (16)$$

where λ_{gi} and λ_c are the heat conduction coefficients of gas species and the catalyst, respectively, which are a function of temperature.

The overall heat transfer coefficients, K_s and K_m account for the heat resistances due to the shell tube and the membrane tube, respectively, and can be given based on the serial resistance model as:

$$K_s = \left(\frac{R_s}{\lambda_s} \cdot \ln(R_{so}/R_s) + \frac{1}{\alpha_s}\right)^{-1} \quad (17)$$

$$K_m = \left(\frac{R_{in}}{R_o + \delta} \cdot \frac{1}{\alpha_s} + \frac{R_{in} \ln(R_o/R_{in})}{\lambda_m} + \frac{1}{\alpha_c}\right)^{-1} \quad (18)$$

where λ_s and λ_m are the heat conduction coefficients of the shell tube and the membrane tube, respectively. The convection heat transport coefficient on the shell side is given by the Dittus–Boelter correlation[16]:

$$\alpha_s = \frac{\lambda_g}{d_e} \cdot 0.023 \left(\frac{d_e \mu_s \rho_g}{\mu_g}\right)^{0.8} \left(\frac{C_p \mu_g}{\lambda_g}\right)^{1/3} \quad (19)$$

where d_e is the equivalent diameter of the fluid cross-sectional area, ($d_e = 2(R_s^2 - R_o^2)/R_s$); u_s is the gas superficial velocity in shell side. For the shell phase, the gas properties in Eq. 19 are obtained based on the air at the shell temperature.

The gas-to-membrane heat transfer coefficient on the catalyst side is evaluated using the following correlation proposed for the packed beds[25]:

$$\frac{\alpha_c d_p}{\lambda_g} = 2 + 1.1\left(\frac{d_p u_t \rho_g}{\mu_g}\right)^{0.6}\left(\frac{C_p \mu_g}{\lambda_g}\right)^{1/3} \tag{20}$$

All the physical properties of gas mixtures in the simulations are calculated at local conditions.[26]

Solution method

The model equations are a group of non-linear partial differential equations and have to be solved numerically. Finite element difference forms in the radial direction are employed to replace the corresponding partial derivative terms in Eqs. 1 and 3 so as to transform them into a series of ordinary differential equations, e.g.,

$$\frac{\partial c}{\partial r} = \frac{c_{k+1} - c_{k-1}}{2\Delta r}, (0 < k < m) \tag{21a}$$

$$\frac{\partial^2 c}{\partial r^2} = \frac{c_{k+1} - 2c_k + c_{k-1}}{\Delta r^2}, (0 < k < m) \tag{21b}$$

where k is the difference mesh order, m is the total number of difference meshes and Δr is the radial differential distance: $\Delta r = R_m/m$.

As a result, the governing equations would have included $7m + 3$ ordinary differential equations, which can be solved numerically using Runge-Kutta method with variable steps. In this work, m was selected to be 8 to attain a sufficient accuracy. The ODEs are stiff and thus the 'ode23s' subroutine in MATLAB software package was employed in this study for the calculations. Simpson's rule is applied to the integrations where needed.

The reactor performance is evaluated through the CH_4 conversion and the CO selectivity, which were calculated by:

$$X_{CH_4} = \left(1 - \frac{1}{F_{CH_r,0}}\int_0^{R_{in}} N_{CH_4} \cdot 2\pi r dr\right) \times 100\% \tag{22}$$

$$S_{CO} = \frac{\int_0^{R_{in}} N_{CO} \cdot 2\pi r dr}{\int_0^{R_{in}} (N_{CO_2} + N_{CO}) \cdot 2\pi r dr} \times 100\% \tag{23}$$

where $F_{CH_4,0}$ is the methane feed flow rate.

The overall oxygen permeation rate may be obtained from the oxygen concentration changes in the shell phase.

Results and Discussions

The following analyses are based on the LSCF perovskite membrane reactor because the kinetic parameters of oxygen permeation through LSCF, k_f, k_r, and D_v have been obtained from independent experiments[20] as shown in Table 2. For other mixed conducting ceramic membranes, they are assumed to follow a similar mechanism for oxygen permeation but only have different kinetics values. The effectiveness factors of catalyst for POM reactions depend not only on the catalyst particle size but also on the temperature and fluid composition, which are changed in radial and axial directions. For the sake of easy-handling, a pseudo-effectiveness factor independent of local conditions, i.e., $\zeta = 0.01$ is used for all three POM reactions in this work.[16] Other parameters required for simulations including the dimensions of membrane reactor and the operating conditions are summarized in Table 3. The parameters with different values shown in Table 3 will be specified in the respective analyses. The methane conversion, CO selectivity, or yield and the oxygen permeation rate under various conditions will be presented in the following section.

Table 2. Kinetic Parameters for Oxygen Permeation Through LSCF Membrane[20]

Diffusion coefficient of oxygen vacancy, $cm^2\ s^{-1}$	$D_v = 1.58 \times 10^{-2} \exp\left(-\frac{8852.5}{T}\right)$
Forward rate constant of the surface exchange reaction, cm $Pa^{-0.5}\ s^{-1}$	$k_f = 1.854 \times 10^4 \exp\left(-\frac{27291}{T}\right)$
Reverse rate constant of the surface exchange reaction, mol $cm^{-2}\ s^{-1}$	$k_r = 2.07 \times 10^4 \exp\left(-\frac{29023}{T}\right)$

Behaviors of the membrane reactor (MR)

Figure 2 displays the distributions of methane, carbon oxide, and oxygen as well as the temperature profile in the catalyst bed of membrane reactor. It can be seen that the methane feed is depleted as it passes through the membrane reactor, and has almost been used out when it arrives at the outlet of the membrane reactor, while a small amount of unreacted methane is remained at the center of the membrane tube ($r = 0$) (Fig. 2a). As the methane reforming reactions (ii and iii) proceed, the CO concentration increases from the

Table 3. Parameters of the Membrane Reactor and Operating Conditions for General Analysis

Dense shell and porous substrate tube	Al_2O_3
Oxygen permeable membrane	$La_{0.6}Sr_{0.4}Co_{0.2}Fe_{0.8}O_{3-\delta}$
POM catalyst	Ni/Al_2O_3
Effective length of membrane reactor, L	0.6 m
Outer radius of shell tube, R_{so}	0.016 m
Inner radius of shell tube, R_s	0.014 m
Outer radius of substrate tube, R_o	0.01 m
Inner radius of substrate tube, R_{in}	0.008 m
Thickness of the perovskite membrane, δ	1.0×10^{-5} m
Catalyst particle size, d_p	2.79×10^{-4} m
Catalyst density, ρ_s	1273 kg m^{-3}
Void fraction of catalyst bed, ε_b	0.43
Effectiveness factor, ζ	0.01
Operating temperature, T_{op}	1123 K
Feed temperature, T_{in}	1123 K
Outlet pressure of membrane reactor, p_a	101.3 kPa
Methane feed flow rate, F_{in}	2.98×10^{-4} mol s^{-1}
Air feed flow rate, F_{Air}	2.98×10^{-3} mol s^{-1}

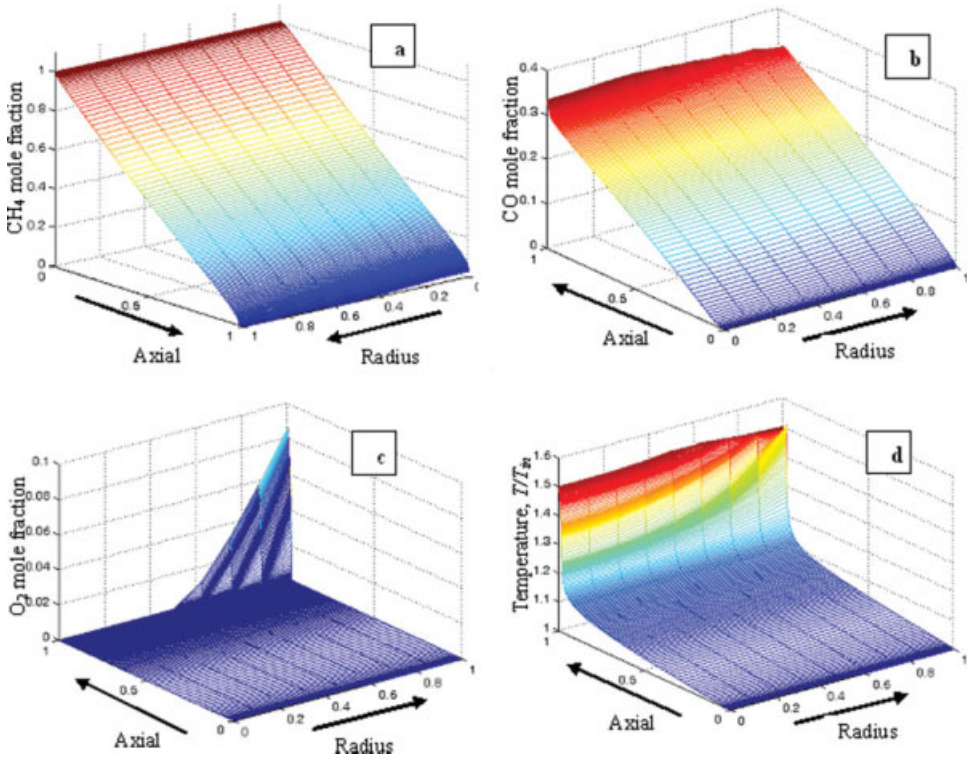

Figure 2. Concentration and temperature profiles in the catalyst bed of tubular membrane reactor.

[Color figure can be viewed in the online issue, which is available at www.interscience.wiley.com.]

inlet to the outlet, and also from the membrane inner surface to the center of the membrane tube (Fig. 2b). The oxygen concentration in most regions of the catalyst bed is close to zero because the oxygen gradually enters into the catalyst bed through the membrane and reacts with the methane of high concentration. At the outlet of membrane tube where the methane has almost been consumed completely, the oxygen concentration increases abruptly (Fig. 2c). Consequently, the CO concentration at the outlet is lowered because of the deep oxidation reaction (Fig. 2b). Because of the net exothermic effect of the POM reactions, the temperature increases mildly along the reactor length in the front part of the membrane tube. But in the region close to the outlet of membrane tube where the methane has nearly been exhausted, a temperature flying phenomenon has occurred, namely, the bed temperature is rapidly increased remarkably due to reactions (Fig. 2d). This is because the methane is firstly oxidized via reaction (i) to release a large amount of heat, but the subsequent endothermic reforming reactions (ii) and (iii) are yet bated since no more methane can be provided after the combustion reaction. At the location where temperature flying begins, the CO selectivity is decreased noticeably, as shown in Figure 2d.

Figure 3 compares the behaviors of the membrane reactor (MR) with the traditional fixed bed reactor (FBR) under the same conditions, where the axial profiles of methane conversion, CO selectivity, temperature averaged in the radial section as well as pressure are plotted. Note that the oxygen feed flow rate for the calculation of FBR is equal to the oxygen permeation rate through the membrane in MR. As can be seen, the methane feed is gradually converted into products in MR, but in FBR the conversion of methane is almost finished instantly as it enters the reactor notwithstanding the product composition, i.e., the CO selectivity may be changed afterwards. The CO selectivity in MR is much higher than that in FBR although it is somewhat reduced in the region close to the reactor outlet, which is caused by the exhaustion of methane. Because of the controlled addition of oxygen by the membrane, the highest temperature or heat point in MR may be much lower than that in FBR. It implies that the excessive temperature excursion causing the catalyst sintering in FBR can be avoided by the use of membrane reactor. Furthermore, although the molar flow rate of syngas product in MR is larger than that in FBR because of the higher CO and H_2 yields, the pressure drop in MR is much lower than that in FBR. This is an additional advantage of the MR over the conventional FBRs.

Effect of operating conditions

It is well known that increasing temperature favors oxygen permeation in the mixed conducting membranes. However, the too high temperature will result in catalyst sintering and deactivation, and is not expected in practical applications. Figure 4 shows the methane conversion, X_{CH4}, CO selectivity, S_{CO} and the oxygen permeation rate as a function of temperature. As is expected, both the methane conversion and oxygen permeation rate increase with increasing the operating temperature. At lower temperatures ($<$1138 K), the methane conversion is lower than 100% and the CO selectivity can be

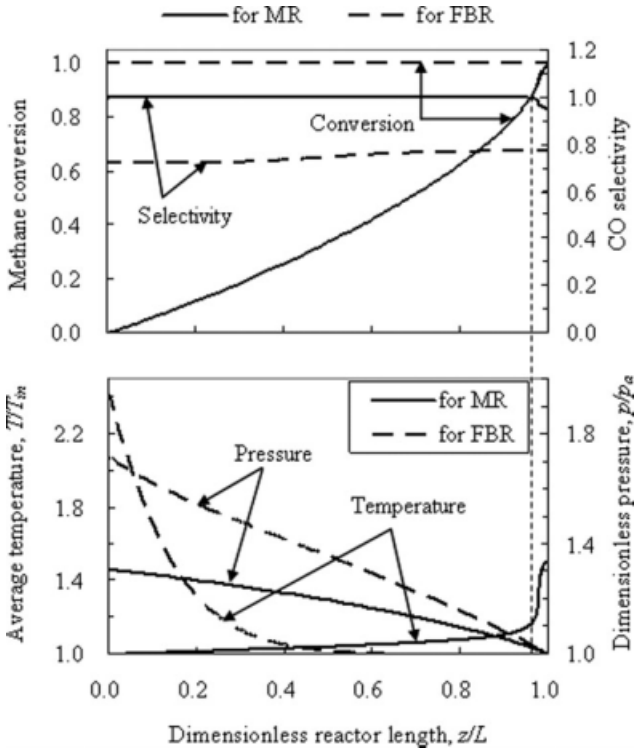

Figure 3. Comparison of membrane reactor (MR) with fixed bed reactor (FBR) in POM performances.

retained close to 100%. As the temperature is increased to 1138 K, the methane conversion approaches to 100% and the CO selectivity decreases rapidly to about 94.7%. The oxygen permeation rate is also remarkably increased at this point because the temperature flying takes place. Nevertheless, further increase in temperature has much less effect on the CO selectivity. This is because as the methane is used up, the oxygen partial pressure on the membrane inside surface would rapidly increase to close to that on the outside surface, causing the oxygen permeation almost to cease. Therefore, the operation of mixed conducting membrane reactors is fairly sensitive to temperature, but a high CO selectivity can always be obtained using membrane reactors.

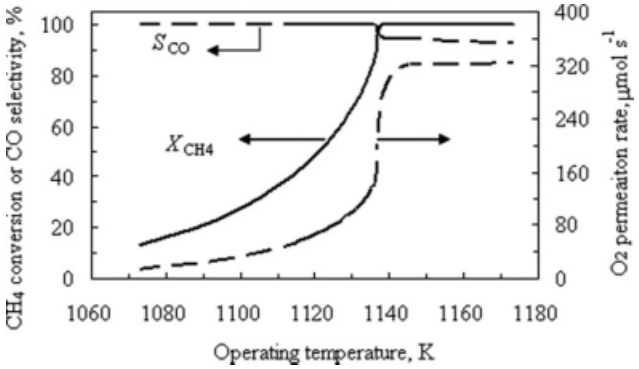

Figure 4. Effect of temperature on the membrane reactor performance.

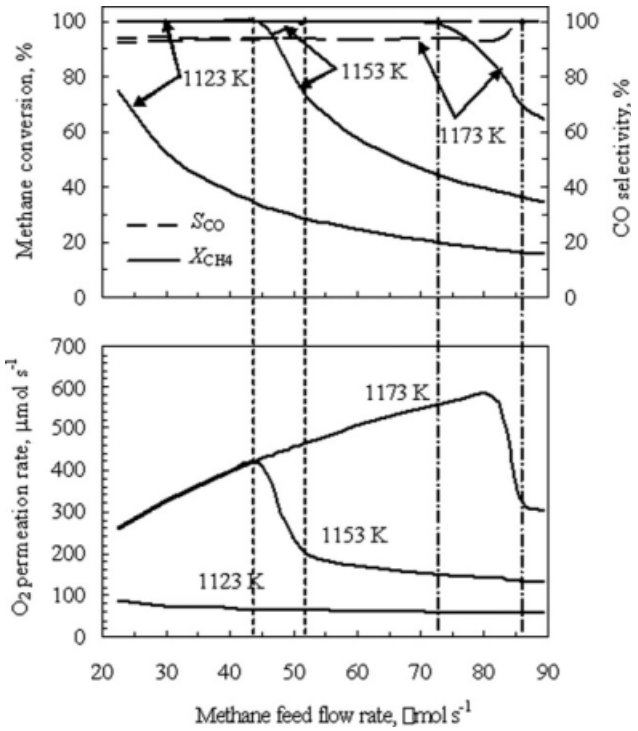

Figure 5. Membrane reactor performances as a function of methane feed flow rate at different temperatures.

Figure 5 plots the methane conversion, CO selectivity and oxygen permeation rate against the methane feed flow rate at different temperatures. At 1123 K, the methane conversion decreases with increasing methane feed flow rate while the CO selectivity is maintained at close to 100% because the methane is not used up. As the temperature is increased to 1153 K, the methane conversion attain up to 100% for the methane feed flow rates of 22–45 μmol s^{-1} while the CO selectivity maintains at around 93%. The higher methane feed flow rate than 45 μmol s^{-1} leads to a lower conversion, but the CO selectivity may approach to 100%. When the temperature is further increased to 1173 K, the methane feed flow

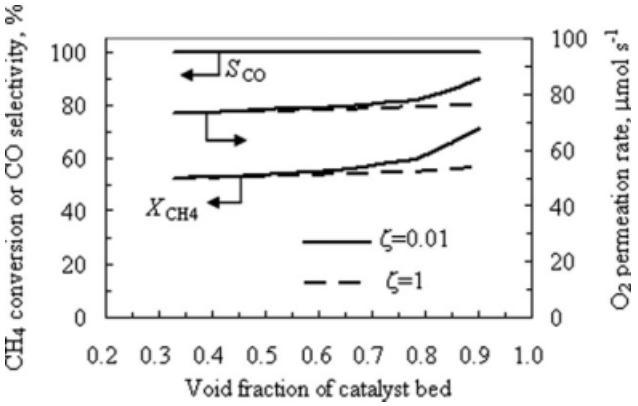

Figure 6. Effect of void fraction of catalyst bed on the membrane reactor performance (the solid lines and dashed lines are for the effectiveness factor of 0.01 and 1, respectively).

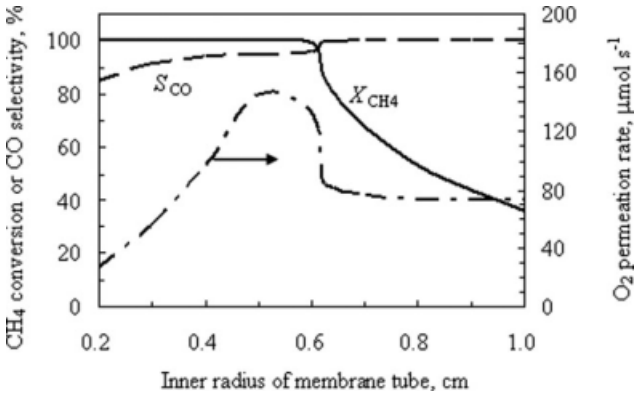

Figure 7. Effect of membrane tube diameter on the reactor performances (wall thickness of tube = 0.2 cm; methane feed velocity = 3.32 cm s^{-1}).

rate corresponding to 100% conversion would increases to 73 μmol s^{-1}. This suggests that the reaction capacity of membrane reactors, which is defined as the maximum methane feed flow rate for complete conversion, may be incremented by increasing temperature. On the other hand, the oxygen permeation rate increases with increasing the methane feed flow rate in the range of complete conversion, but decreases if the methane cannot be used up. As described earlier, the temperature flying only occurs as the methane conversion approaches to 100%, resulting in the remarkable increase in oxygen permeation rate. At lower feed flow rates when the methane can be converted completely, the oxygen permeation rate increases with increasing methane feed flow rate because the oxygen partial pressure on the downstream or the reaction side is decreased. But for the higher feed flow rates at which the methane feed cannot be converted completely, the temperature increment due to the partial oxidation reactions decreases with increasing methane feed flow rate, leading to the decrease in oxygen permeation rate.

Effect of catalyst

Figure 6 illustrates the membrane reactor performance at 1123 K as a function of the void fraction of catalyst bed. It is interesting that the methane conversion increases with increasing the void fraction of catalyst bed. This implies that the methane conversion is not mainly determined by the amount of the catalyst but by the mass transfer in the catalyst bed. As the bed void fraction increases, the oxygen permeated from the air side can enter more easily into the bulk stream to react with methane, leading to higher methane conversion and oxygen permeation rate. On the other hand, the methane conversion decreases as the effectiveness factor of the catalyst is increased from 0.01 to 1, as plotted with the dashed lines in the figure. This unexpected result may be explained as follows. For the POM reactions in mixed conducting membrane reactors, the methane conversion is controlled by the oxygen permeation rate which highly depends on the permeation temperature. As the effectiveness factor all three POM reactions (i), (ii), and (iii) increases, the overall heat released from these reactions would decrease and thus results in the decrease in oxygen permeation rate. These simulation results have given us useful information that the amount of catalyst required for POM in membrane reactors is little and it is better to integrate the catalyst into the porous support so as to minimize hydrodynamic problems, and thus to improve the reactor performance.

Effect of membrane

As described earlier, a high oxygen permeation rate is always required to improve the mixed conducting membrane reactor performance. This can be realized by increasing the membrane area per unit volume, reducing the membrane thickness or by improving the membrane's oxygen permeability. Figure 7 shows the methane conversion, CO selectivity and oxygen permeation rate as a function of the inner radius of the membrane tube, where the membrane wall thickness is kept to be 0.2 cm and the methane feed velocity ($= F_{in}/\pi R_{in}^2$) is kept at 3.32 cm s^{-1}. It can be seen that the methane conversion can reach 100% for the inner radius smaller than 0.6 cm. When the inner radius of membrane tube is larger than 0.6 cm, the methane conversion will decrease remarkably with the CO selectivity approaching to 100% as the inner radius increases. This suggests that the membrane tube larger than 0.6 cm in ID could not provide enough oxygen permeation rate for the POM reactions because of the low ratio of membrane area to reaction volume. For the smaller membrane tubes ($R_{in} < 0.52$ cm), the oxygen permeation rate increases with increasing the membrane radius because both the membrane area for oxygen permeation and the temperature are increased. However, as the membrane inner radius is further increased from 0.52 to 0.62 cm, the oxygen permeation rate would decease noticeably. This is because the temperature flying due to the complete methane conversion has been restrained. Obviously, the smaller membrane tubes, e.g., hollow fiber membranes,[27] should possess much higher POM performances than the larger ones due to the much higher membrane-area/reaction-volume ratio (500–9000 m^2 m^{-3}). Nevertheless, the pressure drop in the packed hollow fiber membranes will be a severe problem that have to be taken into account.

Another method to improve oxygen permeation rate is to reduce the membrane thickness. Figure 8 illustrates the methane conversion, the CO selectivity and the oxygen

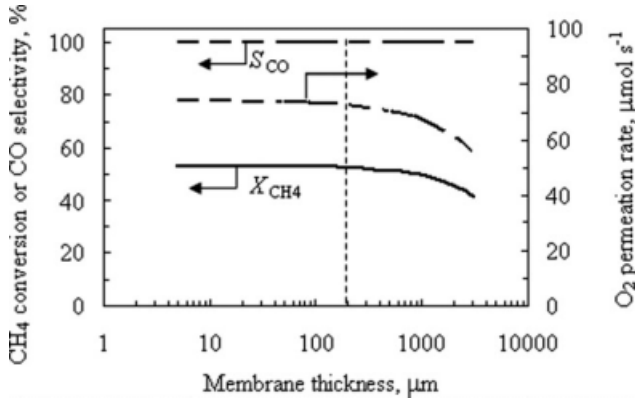

Figure 8. Effect of the thickness of dense membrane on the membrane reactor performance.

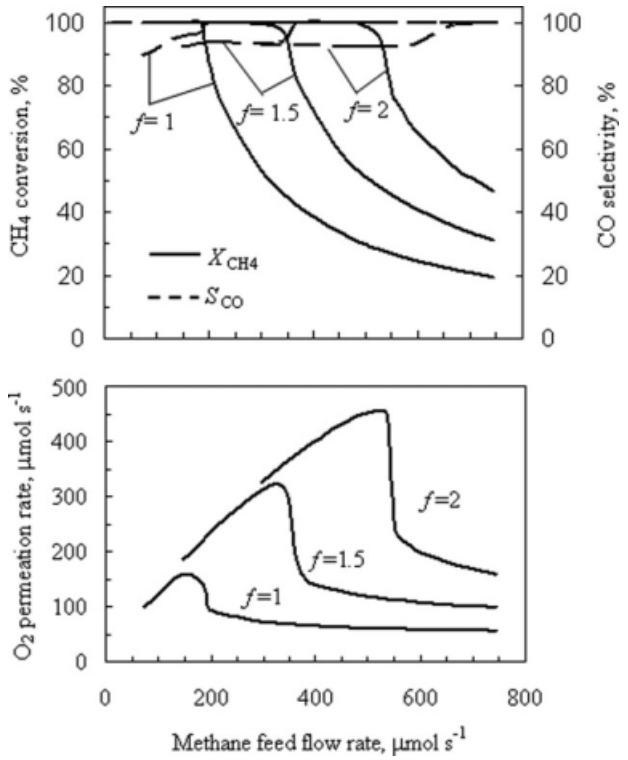

Figure 9. Performances of the membrane reactors with different oxygen permeabilities.

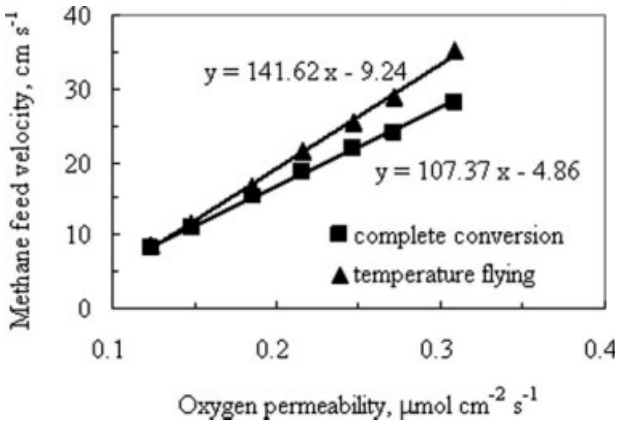

Figure 10. Plot of the operating methane feed velocity against the membranes' oxygen permeability.

permeation rate as a function of the membrane thickness. As is expected, either the oxygen permeation rate or the methane conversion increases as the membrane thickness is decreased. However, when the membrane thickness is lower than 200 μm, the oxygen permeation rate would not increase any longer, and the methane conversion approaches to the maximum 53%. This implies that the oxygen permeation in the LSCF mixed conducting membrane is controlled by the surface exchange kinetics at lower temperatures (i.e. 1123 K). Therefore, for the LSCF membranes the lower membrane thickness (<200 μm) is not necessary for POM at moderate operating temperatures because it cannot bring about obvious increase in methane conversion but lead to a remarkable increase of membrane preparation cost. Comparatively, the surface modification should be a more effective way to improve the membrane reactor performance in POM process.[28]

It has been shown that the methane conversion is largely determined by the oxygen permeability of the mixed conducting membranes. As the LSCF membranes exhibit a low oxygen permeability (2.98×10^{-8} to 1.34×10^{-7} mol cm^{-2} s^{-1})[20] in the POM temperatures of 1073–1173 K, the methane feed velocity allowed by the LSCF membrane reactors is very low. In recent years, considerable researches have been carried out in the development of new mixed conducting membranes such as $Ba_{0.5}Sr_{0.5}Co_{0.2}Fe_{0.8}O_{3-\alpha}$ (BSCF),[29] $La_{0.2}Ba_{0.8}Co_{0.8}Fe_{0.2-x}Zr_xO_{3-\delta}$,[30] and $SrCo_{0.9}Nb_{0.1}O_{3-\delta}$ (SCN),[31,32] which possess much higher oxygen permeability at lower temperatures. Unfortunately, the permeation kinetic expressions for these membranes are not available so far. For the sake of analyses, it is assumed that the permeation expression of Eq. 13 can still be applied to other mixed conducting membranes but only an enhancement coefficient f is multiplied. Figure 9 shows the simulation results for different enhancement coefficients where the methane conversion, CO selectivity and oxygen permeation rate are plotted against the methane feed flow rate. As is expected, the membrane reactor capacity increases with increasing the membrane's oxygen permeability. It also shows that the oxygen permeation rate increases with the methane feed flow rate in the range of complete conversion, decreases remarkably as the methane conversion begins to be less than 100% and deceases tardily at higher feed flow rates. Figure 10 plots the methane feed velocity corresponding to the temperature flying and to the complete conversion,

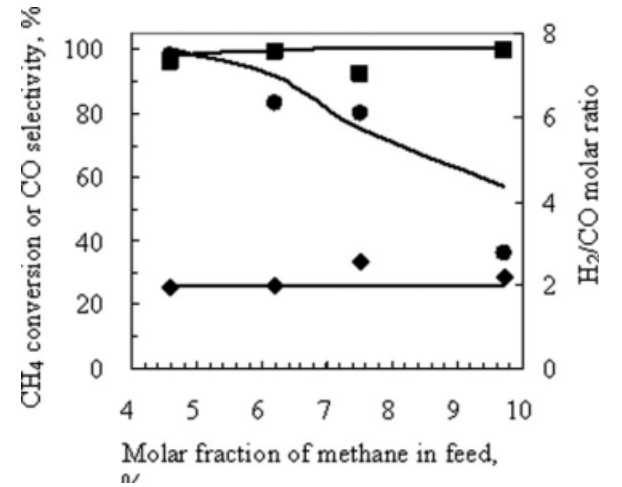

Figure 11. Comparison of simulation results with experimental data (●-methane conversion; ■-CO selectivity; ◆-H_2/CO) (Temperature = 1158 K; Helium flow rate = 4.32×10^{-5} mol s^{-1}; Air flow rate = 7.44×10^{-5} mol s^{-1}; Operating pressures = 0.013 MPa; Bulk density of catalyst bed = 0.726 g cm^{-3}).

respectively against the membrane's oxygen permeability. Based on this figure, the operating methane feed velocity for other mixed conducting membrane reactors can be estimated from their oxygen permeability. For example, since $SrCo_{0.9}Nb_{0.1}O_{3-\delta}$ (SCNb) membrane has an oxygen permeability of 6.69 μmol cm^{-2} s^{-1} at 1173 K,[32] the maximum methane feed velocity for complete conversion in the SCNb membrane reactor can theoretically reach as high as 714.1 cm s^{-1}. However, to avoid temperature flying, the methane feed velocity has to be higher than 939.1 cm s^{-1}. Of course, the practical operating feed velocity may also be affected by other factors such as the dimensions of the membrane reactor.

Comparison with experimental data

Jin et al[7] conducted POM in a LSCF tubular membrane reactor with dimensions of 8 mm in OD, 1.73 cm in effective length and 1.5 mm in membrane thickness. Ni/γ-Al_2O_3 catalyst with the particle sizes of 221 μm and 381 μm (BET surface area ~97.62 m^2 g^{-1}) was packed in the membrane tube. The experimental results for the methane-helium mixture feed are shown in Figure 11 where the methane conversion, H_2/CO ratio and CO selectivity are plotted against the methane fraction in the feed stream. It can be seen that the methane conversion decreases remarkably from about 98% to 36% as the methane feed fraction increases from 4.6 to 9.7%, while the CO selectivity is increased from 96% to close to 100%. All these experimental data are in good agreement with the simulation results by the present model, as shown in the figure. This suggests that the oxygen permeation and the POM kinetic models as well as the parameters used in this study are appropriate for the design of mixed conducting ceramic membranes/membrane reactors.

Conclusions

The performance of mixed conducting ceramic membrane reactors for the POM to syngas has been analyzed using a two dimensional mathematical model. Compared with the conventional FBR, the membrane reactors exhibit many advantages such as a much higher CO selectivity, much lower heating point as well as a much lower pressure drop. However, temperature flying may take place in the membrane reactors as long as the methane feed is converted completely, but can be restrained by increasing the feed flow rate or by lowering the operation temperature. The reaction capacity of the membrane reactors is mainly determined by the oxygen permeation rate rather than by the POM reaction rate on catalyst. To improve the membrane reactor performance, the reduction of mass transfer resistance in the catalyst bed is necessary. Using the smaller membrane tubes is an effective way to achieve a higher reaction capacity because of the higher membrane area/reaction volume ratio, but the pressure drop is a severe problem to be faced. The appropriate operating methane feed velocity for the mixed conducting membrane reactors can be approximately calculated from their oxygen permeability. The experimental data obtained from the LSCF membrane reactor are in good agreement with the modeling results by the present mathematical model.

Acknowledgments

The authors gratefully acknowledge the research funding provided by the National Natural Science Foundation of China (NNSFC, No.20676073), and by EPSRC in the United Kingdom (grant No. EP/F027427/1).

Notation

c_i = concentration of species i, mol m^{-3}
C_{pi} = specific heat capacity of species i, J mol^{-1} K^{-1}
D_{ei} = effective diffusion coefficient of gas i in catalyst bed, m^2 s^{-1}
$D_{i,j}$ = binary diffusion coefficient between species i and j, m^2 s^{-1}
D_V = effective diffusivity of oxygen vacancy, cm^2 s^{-1}
d_e = equivalent diameter of the fluid cross-sectional area, ($d_e = 2(R_s^2 - R_o^2)/R_s$), m
d_p = equivalent diameter of catalyst particle, m
F_i = molar flow rate of species i in the shell phase, mol s^{-1}
F_{Air} = air feed flow rate, mol s^{-1}
$F_{CH_4,0}$ = methane feed flow rate, mol s^{-1}
J_i = permeation flux of species i through membrane, mol m^{-2} s^{-1}
J_h = heat flux due the gas permeation, J m^{-2} s^{-1}
k_j = rate constant for reaction j (j = 1, 2, 3), mol g^{-1} s^{-1} Pa^{-2}
k_f = rate constant for the forward surface exchange reaction, cm Pa$^{-0.5}$ s^{-1}
k_r = rate constant for the reverse surface exchange reaction, mol cm^{-2} s^{-1}
K_i = equilibrium constant for reaction j (j = 1, 2, 3), Pa^2
K_m = overall heat transfer coefficient of membrane tube, W m^{-2} K^{-1}
K_s = overall heat transfer coefficient of shell tube, W m^{-2} K^{-1}
L = effective length of membrane reactor, m
N_i = molar flux of species i in the membrane tube, mol m^{-2} s^{-1}
N_{i0} = molar flux of species i in feed, mol m^{-2} s^{-1}
M = molecular weight of gas m, g mol^{-1}
m = number of difference meshes
p = pressure in catalyst bed, Pa
p_a = pressure at the outlet of membrane reactor or atmospheric pressure, Pa
p' = oxygen partial pressure in the shell phase, Pa
R_{in}, R_o = inner and outer radius of membrane tube, m
R_m = algorithm mean radius of dense membrane, $R_m = \delta/\ln(1 + \delta/R_o)$, m
$\mathcal{R}_j$ = overall rate of reaction j, mol g^{-1} s^{-1}
R = ideal gas constant, 8.314 J mol^{-1} K^{-1}
S = CO Selectivity
T, T' = temperature of the catalyst phase and the shell phase, respectively, K
T_{in}, T_{op} = gas feed temperature and furnace temperature, respectively, K
u_t, u_s = superficial velocity of the lumen gas and the shell gas, respectively, m s^{-1}
X = conversion of methane
y_i = molar fraction of species i

Greek letters

α_s, α_c = gas heat transfer coefficient on the shell or the catalyst side, W m^{-2} K^{-1}
ν_{ji} = stoichiometric coefficient of species i in reaction j
ε_b = void fraction of catalyst bed
ζ_j = effective factor of catalyst for reaction j
δ = thickness of mixed conducting membrane, m
μ_g = gas viscosity, Pa s
ρ_g = gas density, g cm^{-3}
ρ_s = density of catalyst, g cm^{-3}
λ_c = heat conduction coefficient of catalyst, W m^{-1} K^{-1}
λ_{ec} = effective thermal conductivity of tube phase, W m^{-1} K^{-1}
λ_{gi} = heat conduction coefficient of gas species i, W m^{-1} K^{-1}
λ_m = heat conduction coefficient of dense membrane, W m^{-1} K^{-1}
λ_s = heat conduction coefficient of shell tube, W m^{-1} K^{-1}
υ = molecular volume of gas, cm^3 mol^{-1}
ΔH_j = reaction heat of reaction j, J mol^{-1}
Δr = radial differential distance, $\Delta r = R_{in}/m$

Literature Cited

1. Bouwmeester HJM. Dense ceramic membranes for methane conversion. *Catal Today*. 2003;82:141–150.
2. Dong H, Shao Z, Xiong G, Tong J, Sheng S, Yang W. Investigation on POM reaction in a new perovskite membrane reactor. *Catal Today*. 2001;67:3–13.
3. Lu H, Tong J, Cong Y, Yang W. Partial oxidation of methane in $Ba_{0.5}Sr_{0.5}Co_{0.8}Fe_{0.2}O_{3-\delta}$ membrane reactor at high pressures. *Catal Today*. 2005;104:154–159.
4. Ikeguchi M, Mimura T, Sekine Y, Kikuchi E, Matsukata M. Reaction and oxygen permeation studies in $Sm_{0.4}Ba_{0.6}Fe_{0.8}Co_{0.2}O_{3-\delta}$ membrane reactor for partial oxidation of methane to syngas. *Appl Catal A*. 2005;290:212–220.
5. Hu J, Xing T, Jia Q, Hao H, Yang D, Guo Y, Hu X. Methane partial oxidation to syngas in $YBa_2Cu_3O_{7-x}$ membrane reactor. *Appl Catal A*. 2006;306:29–33.
6. Balanchandran U, Dusek JT, Maiya PS, Ma B, Mieville RL, Kleefisch MS, Udovich CA. Ceramic membrane reactor for converting methane to syngas. *Catal Today*. 1997;36:265–272.
7. Jin W, Gu X, Li S, Huang P, Xu N, Shi J. Experimental and simulation study on a catalyst packed tubular dense membrane reactor for partial oxidation of methane to syngas. *Chem Eng Sci*. 2000;55:2617–2625.
8. Zhang W, Smit J, Annaland MS, Kuipers JAM. Experimental and simulation study on a catalyst packed tubular dense membrane reactor for partial oxidation of methane to syngas. *J Membr Sci*. 2007;291:19–32.
9. Caro J, Schiestel T, Werth S, Wang H, Kleinert A, Kölsch P. Perovskite hollow fiber membranes in the partial oxidation of methane to synthesis gas in a membrane reactor. *Desalination*. 2006;199:415–417.
10. Wang H, Tablet C, Schiestel T, Werth S, Caro J. Partial oxidation of methane to syngas in a perovskite hollow fiber membrane reactor. *Catal Commun*. 2006;7:907–912.
11. Ritchie, Richardson JT, Luss D. Ceramic membrane reactor for synthesis gas production. *AIChE J*. 2001;47:2092–2101.
12. Barbieri G, Maio FPD. Simulation of the methane steam re-forming process in a catalytic Pd-membrane reactor. *Ind Eng Chem Res*. 1997;36:2121–2127.
13. Basile A, Paturzo L, Lagana F. The partial oxidation of methane to syngas in a palladium membrane reactor: simulation and experimental studies. *Catal Today*. 2001;67:65–75.
14. Patel KS, Sunol AK. Modeling and simulation of methane steam reforming in a thermally coupled membrane reactor. *Int J Hydrogen Energy*. 2007;32:2344–2358.
15. Rui Z, Zhang K, Li Y, Lin YS. Simulation of methane conversion to syngas in a membrane reactor Part II Model predictions. *Int J Hydrogen Energy*. 2008;33:2501–2506.
16. De Falco M, Di Paola LD, Marrelli L, Nardella P. Simulation of large-scale membrane reformers by a two-dimensional model. *Chem Eng J*. 2007;128:115–125.
17. Hoang DL, Chan SH. Effect of reactor dimensions on the performance of an O_2 pump integrated partial oxidation reformer - a modelling approach. *Int J Hydrogen Energy*. 2006;31:1–12.
18. Ashcroft AT, Cheetham AK, Foord JS, Green MLH, Grey CPJ, Murrell A, Vernon PDF. Selective oxidation of methane to synthesis gas using transition metal catalysis. *Nature*. 1990;344:319–321.
19. Dissanayake D, Rosynek MP, Kharas KCC, Lunsford JH. Partial oxidation of methane to carbon monoxide and hydrogen over a Ni/Al_2O_3 catalyst. *J Catal*. 1991;132:117.
20. Xu SJ, Thomson WJ. Oxygen permeation rates through ion-conducting perovskite membranes. *Chem Eng Sci*. 1999;54:3839.
21. Tan X, Liu S, Li K, Hughes R. Theoretical analysis of ion permeation through mixed conducting membranes and its application to dehydrogenation reactions. *Solid State Ionics*. 2001;138:149–159.
22. Tan X, Li K. Modeling of Air Separation in a LSCF Hollow-Fiber Membrane Module. *AIChE J*. 2002;48:1469–1477.
23. Brunetti A, Caravella A, Barbieri G, Drioli E. Simulation study of water gas shift reaction in a membrane reactor. *J Membr Sci*. 2007;306:329–340.
24. De Falco M, Di Paola L, Marrelli L. Heat transfer and hydrogen permeability in modelling industrial membrane reactors for methane steam reforming. *Int J Hydrogen Energy*. 2007;32:2902–2913.
25. Avci AK, Onsan ZI, Trimm DL. Heterogeneous reactor modeling for simulation of catalytic oxidation and steam reforming of methane. *Chem Eng Sci*. 2001;56:641–649.
26. Reid R, Prausnitz J, Poling B. *The Properties of Gases and Liquid*, 4th ed. New York: McGraw Hill, 1988.
27. Tan X, Liu Y, Li K. Preparation of $La_{0.6}Sr_{0.4}Co_{0.2}Fe_{0.8}O_{3-\alpha}$ hollow fiber membranes for oxygen production by a phase-inversion/sintering technique. *Ind Eng Chem Res*. 2005;44:61–66.
28. Tan X, Wang Z, Liu H, Liu S. Enhancement of oxygen permeation through $La_{0.6}Sr_{0.4}Co_{0.2}Fe_{0.8}O_{3-\delta}$ hollow fibre membranes by surface modifications, *J Membr Sci*. 2008;324:128–135.
29. Liu S, Tan X, Shao ZP, Costa JCD. $Ba_{0.5}Sr_{0.5}Co_{0.8}Fe_{0.2}O_{3-\delta}$ ceramic hollow fiber membranes for air separation. *AIChE J*. 2006;52:3452–3461.
30. Fan CG, Zuo YB, Li JT, Lu JQ, Chen CS, Bae DS. Highly permeable $La_{0.2}Ba_{0.8}Co_{0.8}Fe_{0.2-x}Zr_xO_{3-\delta}$ membranes for oxygen separation. *Sep Purif Technol*. 2007;55:35–39.
31. Nagai T, Ito W, Sakon T. Relationship between cation substitution and stability of perovskite structure in $SrCoO_{3-\delta}$ based mixed conductors. *Solid State Ionics*. 2007;177:3433–3444.
32. Ito W, Nagai T, Sakon T. Oxygen separation from compressed air using a mixed conducting perovskite-type oxide membrane. *Solid State Ionics*. 2007;178:809–816.

Manuscript received July 5, 2008, and revision received Feb. 4, 2009.